Advanced Signal Processing Methods for Ground-Penetrating Radar: Applications to civil engineering

Meng Sun, Jingjing Pan, Cédric Le Bastard, Yide Wang, Jianzhong Li

▶ **To cite this version:**

Meng Sun, Jingjing Pan, Cédric Le Bastard, Yide Wang, Jianzhong Li. Advanced Signal Processing Methods for Ground-Penetrating Radar: Applications to civil engineering. IEEE Signal Processing Magazine, 2019, 36 (4), pp.74-84. 10.1109/MSP.2019.2900454 . hal-02171813

HAL Id: hal-02171813
https://hal.science/hal-02171813

Submitted on 14 Mar 2020

HAL is a multi-disciplinary open access archive for the deposit and dissemination of scientific research documents, whether they are published or not. The documents may come from teaching and research institutions in France or abroad, or from public or private research centers.

L'archive ouverte pluridisciplinaire **HAL**, est destinée au dépôt et à la diffusion de documents scientifiques de niveau recherche, publiés ou non, émanant des établissements d'enseignement et de recherche français ou étrangers, des laboratoires publics ou privés.

Advanced Signal Processing Methods for Ground-Penetrating Radar

Applications to civil engineering

Meng Sun, Jingjing Pan, Cédric Le Bastard, Yide Wang, and Jianzhong Li

Ground-penetrating radar (GPR) is a common technique for evaluating the structure and quality of civil engineering materials. The ever-increasing demand for higher GPR time resolution and better interpretation of GPR data has motivated the use of advanced signal processing methods for GPR applications. In this article, we review the major advances in signal processing techniques employed in civil engineering for different tasks, such as estimation of thickness, permittivity, and roughness. Their performance is tested and compared through numerical testing and using experimental data from laboratory measurements.

Introduction

GPR, employing electromagnetic (EM) waves to survey a variety of media, has numerous applications in many fields [1], [2], such as archeology, civil engineering, agriculture, and the military. In civil engineering, GPR is widely used as a nondestructive testing method to study structures [3] like pavement [4]–[6], buildings [7], and bridges [8]. Figure 1 provides an example of GPR (in particular, step-frequency GPR) in a pavement survey. However, it is not easy to distinguish small targets [5] or to interpret GPR data from very close objects [1], [2] because of the limited time resolution of conventional GPR methods and the complex conditions of the probed media. To improve GPR performance and offer better data interpretation, many signal processing techniques have been proposed [4], [5], [7], [10]–[19] in recent decades. These methods can be divided into two main categories:

- *Basic data processing*: Advanced signal processing methods cannot be applied directly to raw GPR data without basic data processing, such as data editing, filtering, data whitening, and time-zero correction. Generally, these steps should be applied before data interpretation and target detection. These basic data processing methods have been intensively discussed as fundamental knowledge in GPR societies [1], [2], [4].
- *Advanced signal processing methods with preprocessed data*: This is the main focus of this article. Different tasks

(e.g., parameter estimation and imaging) require different signal processing techniques. For conventional GPR, the main data processing difficulty lies in the detection of close backscattered echoes due to the limited time resolution. To improve GPR time resolution [5] and the detection of healthy and damaged zones (interface debonding, etc.), many signal processing methods have been developed, particularly high-resolution techniques. Media parameters, such as layer thickness [5], [10]–[13], media permittivity [7], [12], [19], and interface roughness [14]–[16] are important in evaluating the structure and quality of civil engineering materials. These parameters allow the characterization of the probed media. In the context of small defects or very close interfaces, the parameters cannot be obtained directly from data without specific signal processing methods.

With the technical advancement and rapid development of computer science, GPR techniques have come to achieve fruitful results. Some new signal processing procedures are proposed for GPR systems, such as machine-learning methods and compressive sensing (CS)-based approaches, which have been widely adopted in media parameter estimation and object detection.

Signal model

In civil engineering, GPR applies EM waves to probe the structure and properties of materials in buildings and pavement. The received signals are usually formulated in the frequency domain, such that spectral analysis techniques can be used to estimate the probed media structure. In the far-field condition, the received signal model in the frequency domain can be expressed as [1], [2], [5], [7], [15]

$$r(f_i) = \sum_{k=1}^{K} e(f_i) s_k(f_i) \exp(-j2\pi f_i t_k) + n(f_i), \qquad (1)$$

where K is the number of backscattered echoes; $e(f_i)$ is the radar pulse in the frequency domain; t_k is the time arrival of the kth echo; $n(f_i)$ is an additive white Gaussian noise, with zero mean and variance σ_n^2; and $s_k(f_i) = s_k w_k(f_i)$, where s_k represents the amplitude of the kth backscattered echo under ideal conditions (lossless media with smooth interfaces) and $w_k(f_i) = \alpha_k(f_i) + j\beta_k(f_i)$ represents the complex frequency behavior of the kth backscattered echo at frequency f_i due to the media dispersion or interface roughness. The functions $\alpha_k(f_i)$ and $\beta_k(f_i)$ are nonlinear and depend on the studied media.

For low-loss media like the first two or three pavement layers, the dispersivity can be neglected, according to the work in [1] and [2]. As a consequence, the backscattered echoes are simply time-shifted and attenuated copies of the transmitted signal [5]. With smooth interfaces, the amplitude of the kth backscattered echo is independent of frequency $s_k(f) = s_k$. If the interface roughness is taken into account, the amplitude of the kth backscattered echo decreases with frequency, which can be expressed as $s_k(f) = s_k \alpha_k(f)$ with $\alpha_k(f) < 1$ because of the scattering [15]. For lossy and dispersive media, with the frequency behavior of the kth backscattered echo $w_k(f) = \alpha_k(f) + j\beta_k(f)$, a more sophisticated EM model, such as the constant-Q model, was proposed in [7].

The frequency f can be discretized as $f_i = f_1 + (i-1)\Delta f$ $(i = 1, 2, \ldots, N)$, with N being the number of used frequencies, f_1 the lowest frequency of the used frequency band, and Δf the frequency step. Therefore, (1) can also be written in the following vector form:

$$\mathbf{r} = \mathbf{\Lambda A s} + \mathbf{n} \qquad (2)$$

with the following notational definitions:

- $\mathbf{r} = [r(f_1)\, r(f_2) \ldots r(f_N)]^T$ is the $N \times 1$ received signal vector, called the *observation vector*, which may represent either the measurements by a step-frequency radar or the Fourier transform of an impulse GPR signal; the superscript T denotes the transpose operation.
- $\mathbf{\Lambda} = \text{diag}\{e(f_1), e(f_2), \ldots, e(f_N)\}$ is an $N \times N$ diagonal matrix whose diagonal elements are the radar pulse in the frequency domain.
- $\mathbf{A} = [\mathbf{W}_1 \mathbf{a}(t_1)\, \mathbf{W}_2 \mathbf{a}(t_2) \ldots \mathbf{W}_K \mathbf{a}(t_K)]$ is the $N \times K$ mode matrix.
- $\mathbf{a}(t_k) = [e^{-2j\pi f_1 t_k}\, e^{-2j\pi f_2 t_k} \cdots e^{-2j\pi f_N t_k}]^T$ is the $N \times 1$ mode vector.
- $\mathbf{W}_k = \text{diag}\{w_k(f_1), w_k(f_2), \ldots, w_k(f_N)\}$ is an $N \times N$ diagonal matrix, whose diagonal elements represent the complex frequency behavior of the kth backscattered echo.
- $\mathbf{s} = [s_1\, s_2 \ldots s_K]^T$ is the $K \times 1$ vector of the amplitudes of echoes from lossless media with smooth interfaces.
- $\mathbf{n} = [n(f_1)\, n(f_2) \ldots n(f_N)]^T$ is the $N \times 1$ complex noise vector with zero mean and covariance matrix $\sigma_n^2 \mathbf{I}_N$, and $\mathbf{I}_N$ is the identity matrix of dimension $N \times N$.

Assuming the noise to be independent of the echoes, we can write the data covariance matrix $\mathbf{Y}$ as

$$\mathbf{Y} = E(\mathbf{r}\mathbf{r}^H) = \mathbf{\Lambda A S A}^H \mathbf{\Lambda}^H + \sigma_n^2 \mathbf{I}_N, \qquad (3)$$

where $E(.)$ denotes the ensemble average, $\mathbf{S}$ is the $K \times K$-dimensional covariance matrix of vector $\mathbf{s}$, and superscript H denotes the conjugate transpose operation. With the

FIGURE 1. The French Research Institute of Science and Technology for Transport, Development, and Networks' (IFSTTAR's) air-coupled step-frequency GPR and the automated bench to scan the near subsurface [14].

aforementioned signal model (1), the following steps are the data interpretation and media parameter estimation by signal processing techniques.

Preprocessing techniques

In recent decades, signal processing in GPR applications has achieved a great deal; however, without good-quality data, no methods perform well. Hence, some specific preprocessing techniques must be applied to improve the quality of GPR data to make their interpretation easier. In this section, basic data processing methods and subband averaging techniques are presented.

Basic data processing

Basic GPR data processing methods are usually applied to raw data to better visualize or interpret the GPR data. In most cases, they are mandatory for the subsequent advanced signal processing methods. There are many different types of basic data processing techniques; discussed next are the five most frequently used.

- *Data editing*: This procedure involves the adjustment of the collected raw data by removing and correcting bad data and sorting data files; its purpose is to control the data quality and to give a good interpretation of GPR signals, particularly for GPR measurements in large data volumes, such as pavement surveys [1], [2].
- *Time-zero correction*: The time-zero point is defined as the reference time point corresponding to the air/ground wave first arrival time. However, this point is unstable due to temperature, cable length, and antenna height. The time-zero correction aims at fixing a unique starting point for GPR to measure the time of arrival of echoes [1], [2].
- *Filtering*: The goal of this procedure is to eliminate the echoes received outside the GPR main working time window, such as the multiple reflected echoes outside the time window and direct wave in air. This procedure can help to improve the quality of GPR data.
- *Data whitening*: This operation is to whiten the GPR data by radar pulse [1], [2]. The radar pulse can be measured as the backscattered echo from a metallic plane. After the whitening procedure, the new observation vector $\mathbf{r}'$ can be written as $\mathbf{r}' = \mathbf{\Lambda}^{-1}\mathbf{r} = \mathbf{As} + \mathbf{\Lambda}^{-1}\mathbf{n} = \mathbf{As} + \mathbf{b}$, with $\mathbf{b}$ the new noise vector after the original received data are divided by the pulse. The new covariance matrix $\mathbf{R}$ can be written as

$$\mathbf{R} = E(\mathbf{r}'\mathbf{r}'^{H}) = \mathbf{\Lambda}^{-1}\mathbf{Y}\mathbf{\Lambda}^{-H} = \mathbf{ASA}^{H} + \sigma_n^2\Sigma, \qquad (4)$$

where $\Sigma = \mathbf{\Lambda}^{-1}\mathbf{\Lambda}^{-H} = \text{diag}\left\{\frac{1}{|e(f_1)|^2}, \frac{1}{|e(f_2)|^2}, \cdots, \frac{1}{|e(f_N)|^2}\right\}$.

- *Denoising*: The denoising procedure aims to provide a good interpretation of data by reducing the noise impact on GPR signals. This kind of method is applied by either estimating the power of the noise [20] or utilizing signal enhancement techniques [21].

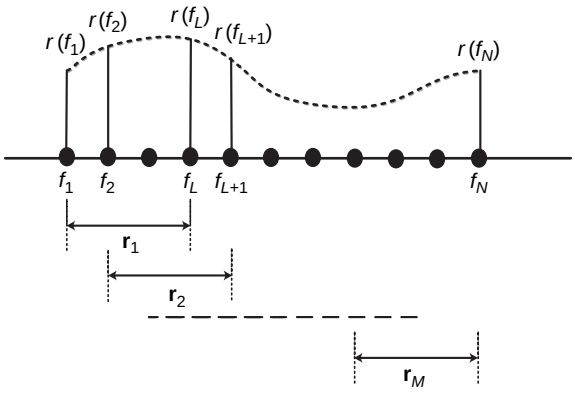

FIGURE 2. The set of the overlapping frequency subbands for the subband averaging techniques.

Subband averaging techniques

In practical environments, the backscattered echoes come from the signal emitted by the transmitter, though usually along different paths. Therefore, these backscattered echoes are highly correlated or even coherent. Consequently, there will be a rank loss of the data covariance matrix. Signal processing methods, such as high-resolution approaches based on the data covariance matrix, suffer greatly from performance degradation due to a mix of signal and noise subspaces. To handle the correlated echoes, the data covariance matrix should be processed with a decorrelation technique, such as subband averaging, which allows the obtaining of a new covariance matrix with a restored rank. With the signal model of low-loss media and smooth interfaces [a frequency behavior of $w(f) \approx 1$], the echoes can be efficiently decorrelated using conventional spatial smoothing preprocessing (SSP) and its extensions, such as modified SSP (MSSP) [17], and the two improved spatial smoothing (ISS) techniques, called *ISSA* [18] and *ISSB* [17] in this article.

As shown in Figure 2, N frequencies and M overlapping subbands with length L are considered. In general, subband averaging techniques work with the following denoised data cross-covariance matrix between the kth subband and the lth subband $\mathbf{R}_{kl}$ (in Figure 2, $\mathbf{r}$ is used instead of $\mathbf{r}'$):

$$\mathbf{R}_{kl} = E(\mathbf{r}'_k\mathbf{r}'^{H}_l) = \mathbf{A}_L\mathbf{D}^{k-1}\mathbf{S}(\mathbf{D}^{l-1})^{H}\mathbf{A}_L^{H}, \qquad (5)$$

where $\mathbf{r}'_k$ and $\mathbf{r}'_l$ denote the $L \times 1$ data vector of the kth and lth subbands, respectively. $\mathbf{A}_L$, corresponding to the first L rows of matrix $\mathbf{A}$, is the $L \times K$ mode matrix, which is independent of parameter k, and $\mathbf{D}$ denotes the $K \times K$ diagonal matrix, expressed as $\mathbf{D} = \text{diag}\{e^{-2j\pi\Delta f t_1}, \ldots, e^{-2j\pi\Delta f t_K}\}$.

Table 1 and Figure 3 summarize the principle and performance of the subband averaging techniques. We can see from Table 1 that ISSB takes advantage of both the cross subband covariance matrices $\mathbf{R}_{kl}$ and the covariance matrices $\mathbf{R}_{kk}/\mathbf{R}_{ll}$, unlike SSP, MSSP, and ISSA, which exploit only the covariance matrices $\mathbf{R}_{kk}/\mathbf{R}_{ll}$. Therefore, by using more data to estimate the rank-restored data covariance matrix, ISSB is more powerful for decorrelation than SSP, MSSP, and ISSA. This

is confirmed in Figure 3, where we have calculated the relative root-mean-square error (RRMSE) of the estimated time delay by ESPRIT with SSP, MSSP, ISSA, and ISSB. Among these methods, ISSB provides the best performance with the smallest RRMSE in the scenario of the tested signal-to-noise ratios (SNRs). The computational complexity of the subband averaging techniques is also mentioned in Table 1; the computational load of ISS techniques is slightly higher than that of the conventional SSP and MSSP.

Advanced signal processing methods for GPR applications

After using preprocessing techniques, advanced signal processing methods can be applied. The objectives of the latter employed on GPR data are 1) to improve the GPR time resolution and 2) better estimate the parameters of the surveyed media.

Regarding the first purpose, the GPR processing time resolution is defined by the $B\Delta\tau$ product for a given frequency band B as the minimal time shift $\Delta\tau$ between two echoes that the processing is able to distinguish [5]. Indeed, the limit resolution of classical GPR is $B\Delta\tau = 1$. Figure 4 provides an example of classical GPR time resolution with different $B\Delta\tau$ products. As shown in Figure 4, classical GPR cannot directly resolve echoes for a $B\Delta\tau$ product smaller than one. In the literature, there are two possible solutions for increasing the resolution. One is to increase the frequency bandwidth of the GPR. For example, the time delay is smaller than 0.2 ns for echoes coming from two smooth interfaces of homogeneous media having a thickness of 2 cm and a relative permittivity of five. As such, a GPR with a frequency bandwidth larger than 5 GHz is required to distinguish them. Another solution is to apply high-resolution signal processing methods to improve the GPR time resolution.

For the second purpose, media parameters like permittivity and interface roughness cannot be recovered directly from data. This fact leads to the development of signal processing methods for media parameter estimation. However, some signal processing techniques, such as high-resolution approaches, suppose that the number of backscattered echoes is known beforehand. Therefore, we first introduce echo detection methods to estimate the number of echoes. Then, some major methods for media parameter estimation are presented.

Echo detection methods

GPR is used to detect the backscattered echoes from the studied media. The amplitudes and phases of the backscattered echoes contain useful information, such as time delays and wave speed, which are important for analyzing the internal structure of civil engineering materials. Furthermore, for high-resolution methods [5] or some machine-learning methods [19], the number of backscattered echoes should be known a priori. However, the number of echoes to be detected is unknown in practice.

Methods have been proposed for echo detection, such as Akaike's information criterion (AIC) and minimum description

Table 1. A summary of the subband averaging techniques (J is the $L \times L$ exchange matrix, and the operator * denotes the complex conjugate).

Method	Averaged Data Covariance Matrix	Computational Complexity
SSP	$\mathbf{R}_{SSP} = \frac{1}{M}\sum_{k=1}^{M}\mathbf{R}_{kk}$	$O(ML^2)$
MSSP	$\mathbf{R}_{MSSP} = \frac{1}{2M}\sum_{k=1}^{M}\{\mathbf{R}_{kk} + \mathbf{J}\mathbf{R}_{kk}^{*}\mathbf{J}\}$	$O(ML^2)$
ISSA	$\mathbf{R}_{ISSA} = \frac{1}{2M}\sum_{k=1}^{M}\sum_{l=1}^{M}\{\mathbf{R}_{kk}\mathbf{R}_{ll} + \mathbf{J}\mathbf{R}_{kk}^{*}\mathbf{R}_{ll}^{*}\mathbf{J}\}$	$O(M^2L^3)$
ISSB	$\mathbf{R}_{ISSB} = \frac{1}{2M}\sum_{k=1}^{M}\sum_{l=1}^{M}\{\mathbf{R}_{kl}\mathbf{R}_{lk} + \mathbf{J}\mathbf{R}_{kl}^{*}\mathbf{R}_{lk}^{*}\mathbf{J}\}$	$O(M^2L^3)$

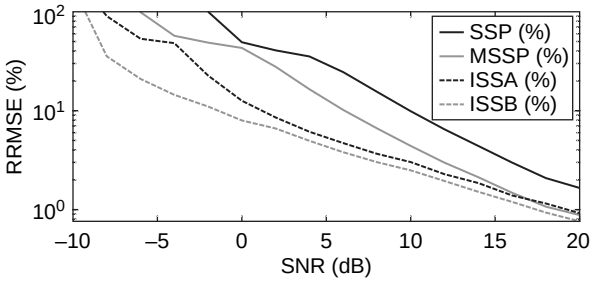

FIGURE 3. The relative root-mean-square error (RRMSE) of the estimated time delay between two echoes versus the signal-to-noise ratio (SNR) by ESPRIT with SSP, MSSP, ISSA, and ISSB. The true time delay is 0.3 ns, and the frequency bandwidth $B = 2$ GHz, with 1,000 independent Monte Carlo process runs.

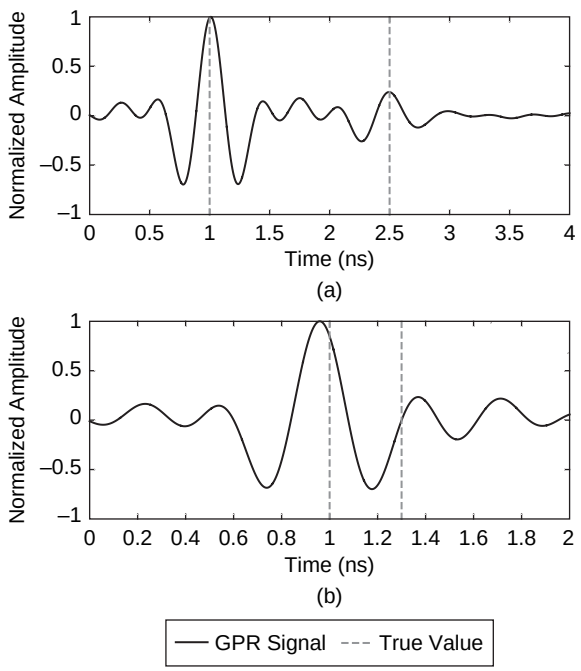

FIGURE 4. The GPR signals at SNR = 20 dB and B = 2 GHz: (a) nonoverlapped echoes $B\Delta\tau = 3$; (b) overlapped echoes $B\Delta\tau = 0.6$.

length (MDL) [22], which are based on eigenvalue decomposition (EVD) of the data covariance matrix and information-theoretic criteria. The merit of AIC and MDL is that they do not require any subjective threshold setting but estimate the number of echoes in an objective way. The number of echoes can be determined by searching the minimum value of the following AIC and MDL criteria:

$$K = \min_i [C(i)], \tag{6}$$

where $C(i)$ $(i = 0, 1, ..., L-1)$ is the cost function of AIC and MDL, given by the equation appearing in the box at the bottom of this page, where λ_j is the jth eigenvalue of the data covariance matrix (arranged in decreasing order) after subband averaging techniques, with $j = 1, 2, ..., L$; and N_x is the number of snapshots. However, as mentioned in [23] and [24], AIC tends to asymptotically overestimate the number of echoes, while MDL performs poorly at low SNRs or a limited number of snapshots (leading to an underestimation of the number of echoes). To solve the problems coming from low SNRs as well as a limited number of snapshots, numerous adaptations of AIC and MDL have been proposed [23], [24]. With the knowledge of the number of echoes, media parameter estimation methods are introduced in the following section.

Thickness estimation in low-loss media

Over the past several decades, many signal processing techniques have been proposed for thickness estimation with low-loss media and smooth interfaces [10]–[13], especially small thicknesses [5]. As previously mentioned, for such interfaces, the frequency behavior $w(f) \approx 1$. For horizontally stratified media like pavement, the layer thickness H can be deduced from the time delay $\Delta\tau$ between two backscattered echoes associated with each interface and the relative permittivity ε_r of the media, as follows:

$$H = \frac{c\Delta\tau}{2\sqrt{\varepsilon_r}}, \tag{7}$$

where c is the speed of light. Therefore, estimating thickness is equivalent to retrieving the time delay of echoes and the relative permittivity of each layer. In the following, we will review three types of time-delay estimation (TDE) methods: the high-resolution method, machine-learning method, and CS-based method.

High-resolution approaches

Subspace-based high-resolution methods

Such techniques were originally proposed for the direction-of-arrival detection of incoming plane waves using an array of sensors and have lately been successfully developed for spectral analysis and thickness estimation (employing time delays and media permittivity). These algorithms are based on the eigenstructure properties of the data covariance matrix. They are known for their high-resolution ability and excellent estimation accuracy as compared to the conventional fast Fourier transform-based methods. The two most prominent subspace-based methods—MUSIC and ESPRIT [5]—are presented here for TDE.

- ***MUSIC***: The MUSIC algorithm is based on the orthogonality of signal and noise subspaces. The preprocessed data covariance matrix $\mathbf{R}_x$, after undergoing whitening, denoising, and subband averaging, can be written in terms of its eigenvalues and eigenvectors as

$$\mathbf{R}_x = \mathbf{U}_S \mathbf{\Lambda}_S \mathbf{U}_S^H + \mathbf{U}_N \mathbf{\Lambda}_N \mathbf{U}_N^H, \tag{8}$$

  where subscript x represents the selected subband averaging technique; $\mathbf{\Lambda}_S$ is a diagonal matrix containing the K largest eigenvalues, with their associated eigenvectors in the columns of $\mathbf{U}_S$ (the matrix of signal eigenvectors); and $\mathbf{\Lambda}_N$ is a diagonal matrix containing the $L-K$ smallest eigenvalues, with their associated eigenvectors arranged in $\mathbf{U}_N$ (the matrix of noise eigenvectors). The MUSIC principle is based on the fact that $\mathbf{U}_N$ is orthogonal to $\mathbf{U}_S$ and, consequently, to the mode matrix $\mathbf{A}_L$ $(\mathbf{U}_N^H \mathbf{a}_L(t_k) = 0, k = 1, ..., K)$. The MUSIC pseudospectrum can be written as

$$P_{\text{MUSIC}}(t) = \frac{1}{\mathbf{a}_L^H(t)\mathbf{U}_N\mathbf{U}_N^H\mathbf{a}_L(t)}. \tag{9}$$

  The time delays can be estimated by searching the peak positions of $P_{\text{MUSIC}}(t)$.
- ***ESPRIT***: The MUSIC algorithm requires a 1D search for parameter estimation. Compared to MUSIC, ESPRIT affords direct parameter estimation with lower computational complexity. It divides the mode matrix $\mathbf{A}_L$ into two overlapping submatrices:

$$C(i) = \begin{cases} -2N_x(L-i)\log\left\{\dfrac{\prod_{j=i+1}^{L}\lambda_j^{1/(L-i)}}{1/(L-i)\sum_{j=i+1}^{L}\lambda_j}\right\} + 2i(2L-i) & \text{AIC} \\ -N_x(L-i)\log\left\{\dfrac{\prod_{j=i+1}^{L}\lambda_j^{1/(L-i)}}{1/(L-i)\sum_{j=i+1}^{L}\lambda_j}\right\} + 0.5i(2L-i)\log N_x & \text{MDL} \end{cases},$$

$$\mathbf{A}_L = \begin{pmatrix} \mathbf{A}_{L1} \\ - \end{pmatrix} = \begin{pmatrix} - \\ \mathbf{A}_{L2} \end{pmatrix}.$$

The $(L-1)\times K$-dimensional mode matrices of each subband $\mathbf{A}_{L1}$ and $\mathbf{A}_{L2}$ are related to each other by the $K\times K$ diagonal matrix $\mathbf{D}$ defined in the "Subband Averaging Techniques" section, the diagonal elements of which depend on the time delay to be estimated. The relationship between $\mathbf{A}_{L1}$, $\mathbf{A}_{L2}$, and $\mathbf{D}$ can be expressed as

$$\mathbf{A}_{L2} = \mathbf{A}_{L1}\mathbf{D}. \tag{10}$$

However, matrix $\mathbf{D}$ cannot be directly estimated from data; thus, we need to find a way to estimate the diagonal elements of $\mathbf{D}$. According to [5], based on the EVD of the data covariance matrix $\mathbf{R}_x$, the diagonal elements of $\mathbf{D}$ can be retrieved from a similar matrix that has the same eigenvalues as $\mathbf{D}$. As such, the time delay can be estimated by calculating the phase of the eigenvalues of this new matrix.

High-resolution methods without EVD

The subspace-based methods require EVD or singular-value decomposition (SVD), which involve a large computational burden. To solve this problem, the propagator-based methods or linear subspace methods, such as the orthogonal propagator method (OPM) [25], are proposed to estimate the time delay by using linear operations without EVD or SVD. In the following, the principle of the OPM applied for TDE is briefly recalled.

The OPM is based on the structure of the data covariance matrix $\mathbf{R}_x$, which partitions matrix $\mathbf{A}_L$ into two submatrices:

$$\mathbf{A}_L = \begin{pmatrix} \mathbf{A}_L\uparrow \\ \mathbf{A}_L\downarrow \end{pmatrix},$$

where $\mathbf{A}_L\uparrow$ and $\mathbf{A}_L\downarrow$ are $K\times K$ and $(L-K)\times K$-dimensional matrices, respectively. There exists a $K\times(L-K)$-dimensional linear operator $\mathbf{P}$, such that $\mathbf{P}^H\mathbf{A}_L\uparrow = \mathbf{A}_L\downarrow$ or $[\mathbf{P}^H, -\mathbf{I}_{L-K}]\mathbf{A}_L = \mathbf{Q}^H\mathbf{A}_L = \mathbf{0}$, where $\mathbf{I}_{L-K}$ is an $(L-K)\times(L-K)$-dimensional identity matrix. Because $\mathbf{A}_L$ is full rank, the linear operator $\mathbf{P}$ is unique. Similar to the idea of subspace-based methods, the mode vectors are orthogonal to the columns of $\mathbf{Q}$ $(\mathbf{Q}^H\mathbf{a}_L(t_k) = 0, k = 1, ..., K)$. Consequently, we can obtain the following OPM pseudospectrum:

$$P_{\mathrm{OPM}}(t) = \frac{1}{\mathbf{a}_L^H(t)\mathbf{Q}(\mathbf{Q}^H\mathbf{Q})^{-1}\mathbf{Q}^H\mathbf{a}_L(t)}. \tag{11}$$

The time delays of the echoes can then be estimated by searching the peak positions of (11). The propagator $\mathbf{P}$ is unknown in reality, which can be retrieved from the structure of the data covariance matrix $\mathbf{R}_x$ [25]. Unlike subspace-based methods, which use EVD to calculate U_N, the propagator estimation can be done without EVD, which is computationally efficient. However, propagator-based methods are developed with signal models under ideal conditions and without the consideration of noise. Hence, their performance is degraded in low-SNR scenarios.

Machine learning

In recent years, there has been a boom in machine-learning techniques for parameter estimation in many domains. Here, machine-learning applications are classified into two categories: supervised learning and combined methods (where machine-learning and signal processing techniques are integrated).

Supervised learning

The classical machine-learning approaches with GPR systems are based on the supervised-learning process. The purpose of supervised learning is to approximate the mapping from the inputs to the outputs, as shown in Figure 5. The inputs are the feature representations of the GPR data, for example, the elements of the data covariance matrix, $\mathbf{v} = [\mathbf{R}(1,1), \mathbf{R}(1,2), \ldots, \mathbf{R}(N,N)]^T$ [19]. The outputs are the parameters to be estimated (time delay, roughness, permittivity, and so forth). The mapping can be either linear or nonlinear while the latter might depend on kernel-based mechanisms to deal with the nonlinear data. This process requires learning databases. Then the approximated mapping can work automatically on new inputs, which is also known as *testing*. The most frequently used supervised-learning algorithms in parameter estimation include support vector regression (SVR) [19], [26] and neural networks.

SVR is the regression form of the support vector machine. It is based on the structural risk minimization principle, which takes both the structural and empirical errors of the model into account. It has a good generalization ability, even in small sample learning problems. In TDE [19], the case of K echoes is considered. K sets of training data are applied, and the feature vector $\mathbf{v}$ is normalized to obtain the vector $\mathbf{z}$, with $\mathbf{z} = (\mathbf{v}/\|\mathbf{v}\|)$. The kth set of training data is expressed as $[(\mathbf{z}_k^0, t_k^0), (\mathbf{z}_k^1, t_k^1), \ldots, (\mathbf{z}_k^{N_p-1}, t_k^{N_p-1})]$, with N_p being the number of training pairs. The regression function in TDE is, therefore, $f(\mathbf{z}) = \langle \mathbf{w}, \mathbf{z} \rangle + b$, with $\langle . \rangle$ the inner product. $\mathbf{w}$ and b are the regression parameters, which are determined by an optimization problem. Consequently, the time delays can be estimated according to the regression function.

Combined methods

There is also a group of applications that marries machine-learning and signal processing approaches, namely, the combined

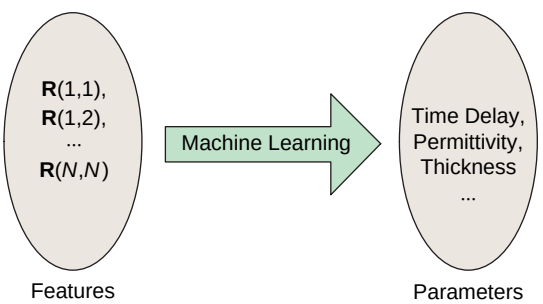

FIGURE 5. The principle of the supervised-learning process.

methods, such as SVR-based linear prediction (LP) or forward-backward LP (FBLP)-SVR in [10]. Unlike the supervised-learning applications, the key insight of the combined techniques is to find the solution of signal processing approaches under the concept of machine-learning theory. As it turns out, the combined methods exploit machine learning but also extend the original signal processing algorithms with enhanced accuracy and robustness. For example, the LP-based methods try to find the relationship between the next GPR signal $\mathbf{y}$ and its previous observation $\mathbf{Z}$:

$$\mathbf{Z}\omega = \mathbf{y}, \tag{12}$$

where ω is the weighting coefficient vector. The conventional LP method calculates ω by using the least-squares approach $\omega = (\mathbf{Z}^H\mathbf{Z})^{-1}\mathbf{Z}^H y$, but with constraints on the number of observations. Different from the conventional LP solution, (12) can be viewed as a typical SVR problem in the complex domain [10]; therefore, ω can be estimated by the SVR principle. In [10], the combined LP–SVR performs well in the case of both coherent echoes and limited snapshots. However, its computational load is a little higher than those of the conventional LP method.

CS

It has been previously mentioned that the GPR echoes may be coherent, which would lead to a rank loss of the data covariance matrix. Therefore, the aforementioned high-resolution methods cannot be applied directly without decorrelation techniques. In the past decade, new parameter estimation methods based on CS have been proposed that can process the coherent signals with high accuracy [27]–[29].

In TDE, the entire time domain can be sampled with a dictionary matrix, such as $\mathbf{T} = [\tau_0, \tau_1, \ldots, \tau_i, \ldots, \tau_{N_0}]$, with $N_0 \gg K$. If $\mathbf{T}$ is dense enough, K values in $\mathbf{T}$ can be expected to be very close (or even equal) to the true time arrivals t_k, with $k = 1, 2, \ldots, K$; if not, there will be a bias in the TDE. Therefore, the sparse form of the received signal can be written as

$$\mathbf{r}_T = \Lambda\mathbf{A}_T\mathbf{x} + \mathbf{n}, \tag{13}$$

Table 2. A summary of methods (N_t is the number of search points in the time spectrum)

Method	Coherent Signals	Computations	Frequency Behavior $w(f)$
MUSIC	No	$O(L^3 + (2L(L-K) + L)N_t)$	Linear
ESPRIT	No	$O(L^3 + 3(L-1)K^2 + 2K^3)$	Linear
OPM	No	$O(L^2K + (L-K)^2K + (2L(L-K) + L)N_t)$	Linear
Machine learning	Yes	—	Linear/ nonlinear
CS	Yes	—	Linear/ nonlinear

where $\mathbf{A}_T = [\mathbf{a}(\tau_0), \mathbf{a}(\tau_1), \ldots, \mathbf{a}(\tau_i), \ldots, \mathbf{a}(\tau_{N_0})]$ is the $(N \times (N_0 + 1))$-dimensional overcomplete dictionary, and the $(N_0 + 1) \times 1$ vector $\mathbf{x} = [x_0, x_1, \ldots, x_{N_0}]^T$, with only K nonzero elements defined as the sparse form of $\mathbf{s}$. Thus, when $\tau_i = t_k$, we obtain $x_i = s_k$. The most direct way to recover the nonzero value of $\mathbf{x}$ is to minimize the ℓ_0 norm; however, it is an intractable optimization problem. As mentioned in [27] and [28], when vector $\mathbf{x}$ is sparse enough, the ℓ_0 norm can be replaced by the ℓ_1 norm. Vector $\mathbf{x}$ satisfies the sparse condition because of $K \ll N_0$. Therefore, TDE can be achieved by solving the following optimization problem [27], [28]:

$$\hat{\mathbf{x}} = \arg\min_x \left\{ (1-\mu) \left\| \Lambda\mathbf{A}_T\mathbf{x} - \mathbf{r}_T \right\|_2^2 + \mu \left\| \mathbf{x} \right\|_1 \right\}, \tag{14}$$

where $\mu \in [0, 1]$ is the regularization parameter controlling the tradeoff between the quality of fit $\left\| \Lambda\mathbf{A}_T\mathbf{x} - \mathbf{r}_T \right\|_2$ and the degree of sparsity. This parameter is important to the estimation accuracy. The nonzero value of $\mathbf{x}$ can be recovered by using some existing sparse reconstruction methods, such as second-order cone programming (SOCP) [28]. Then, vector $\mathbf{x}$ is rebuilt, and the positions of nonzero elements in $\mathbf{x}$ as well as the corresponding positions in $\mathbf{A}_T$ can be estimated. Consequently, the time delays of the backscattered echoes can be obtained.

With the estimated time delays, the echo amplitudes can be retrieved from the signal model of the low-loss media with smooth interfaces, by

$$\hat{\mathbf{s}} = (\hat{\mathbf{A}}^H\hat{\mathbf{A}})^{-1}\hat{\mathbf{A}}^H\Lambda^{-1}\mathbf{r}, \tag{15}$$

where $\hat{\mathbf{A}}$ is the $N \times K$ mode matrix constructed from the estimated time delays. Then, the relative permittivity of each layer can be deduced [12]. For example, the estimated relative permittivity of the first layer $\hat{\varepsilon}_{r1}$ can be expressed as

$$\hat{\varepsilon}_{r1} = \left(\frac{1 - \hat{s}_1}{1 + \hat{s}_1} \right)^2, \tag{16}$$

where $\hat{s}_1$ represents the estimated amplitude of the first backscattered echo. Therefore, the layer thickness can then be retrieved from the estimated time delays and relative permittivity.

In Table 2, we summarize the characteristics of the previously noted methods for low-loss media. It can be seen that the mentioned high-resolution techniques cannot directly work with coherent signals because of the rank loss of the data covariance matrix, while machine-learning and CS-based methods can handle the case of coherent signals. Then, the major computational requirements of the noted methods are presented. ESPRIT and MUSIC require EVD of the data covariance matrix. In contrast, the OPM does not apply EVD but needs a 1D search in the time spectrum (as with MUSIC). There is no analytical expression to indicate the computational complexity of machine-learning methods, which are black boxes.

Meanwhile, the computational load of CS-based methods is based on the applied sparse reconstruction methods. In addition, when the frequency behavior $w(f) \neq 1$, the methods presented in Table 2 can also be adapted for TDE, but with some modifications. For example, without modifications, MUSIC,

ESPRIT, and the OPM can work only when the exponent of $w(f)$ is a linear function of the frequency. Although machine-learning and CS-based methods can be directly applied when the exponent of $w(f)$ is either a linear or nonlinear function of the frequency, a multidimensional search is required.

Simulation examples

We also present some simulation examples to show the performance of various methods—two subspace-based ones (MUSIC and ESPRIT), a propagator-based method (OPM), one based on machine learning (FBLP-SVR), and a CS-based technique (CS-SOCP). The simulation data represent the radar backscattered echoes from a layer made up of two interfaces separating homogeneous media, as shown in Figure 6. The studied medium consists of a layer of ultrathin asphalt surface with relative permittivity ε_{r1} equal to 4.5, overlying a baseband with relative permittivity ε_{r2} equal to seven; the thickness of layer one is $H \approx 20$ mm, which can be estimated from the TDE of the first two echoes. and the thickness of layer 2 is supposed to be infinite. The frequency bandwidth is 0.5–2.5 GHz, with 0.05-GHz steps (41 frequency samples), and the number of subbands is equal to 20. The dimensions of CS-SOCP overcomplete dictionary $\mathbf{A}_T$ are 41×181; the SNR is defined as the ratio between the power of the second echo and the noise variance.

In the simulation, the performance of the compared algorithms versus the SNR is evaluated by a Monte Carlo process of 100 independent runs with 500 independent snapshots. The SNR varies from 0 to 20 dB. Figure 7 shows the RRMSE of the estimated thickness using different methods. It is clear from Figure 7 that CS-SOCP offers the best performance (with the smallest RRMSE) in thickness estimation. CS-SOCP can handle the coherent signals without subband averaging, which makes use of full frequency bandwidth. Then, the subspace-based methods MUSIC and ESPRIT share similar performance, but with a greater RRMSE than that of CS-SOCP. In low-SNR scenarios, the RRMSE of the OPM is greater than the compared subspace-based methods because it is founded on a noise-free signal model. As the SNR increases, the OPM's performance tends to be similar to that of MUSIC and ESPRIT. The performance of FBLP-SVR is similar to that of the conventional FBLP with large snapshots (>100) but is worse than with the high-resolution methods.

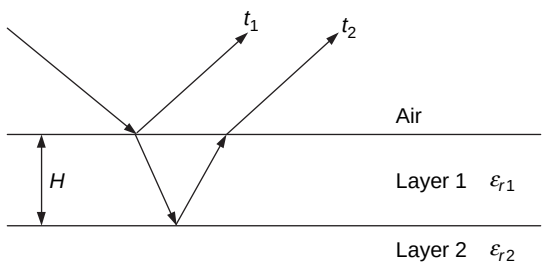

FIGURE 6. The pavement configuration, with t_k representing the time delay of the kth echo.

Moreover, in Table 3, we calculate the consuming time of the compared algorithms for a single run with one snapshot. As expected, the consuming time of CS-SOCP is much higher than the compared high-resolution methods and FBLP-SVR because of the choice of dictionary matrix; and the consuming time of the high-resolution methods confirms the computational loads mentioned in the previous section. In addition, for MUSIC, the OPM, and FBLP-SVR, a 1D search occupies the majority of the consuming time. Some adaptations have been proposed to avoid a 1D search; for example, root-MUSIC [5] estimates the time delay by calculating the roots of the MUSIC cost function.

Interface roughness estimation in low-loss media

At usual GPR wavelengths (the decimeter range in the air), the interface roughness may be neglected. But within the scope of centimeter waves, the influence of the interface roughness must be considered [15]. The interface roughness can produce a particular frequency signature of the echoes' amplitudes, which decrease with frequency [15]. It is only recently that interface roughness estimation has gained more attention, leading to the development of new signal processing methods [14]–[16].

With a frequency band B inferior to 2 GHz, interface roughness estimation can be carried out by taking into account an exponential frequency behavior $w_k(f) = \alpha_k(f) \approx \exp(-b_k f)$, with b_k the roughness parameter of the kth interface [15], [16].

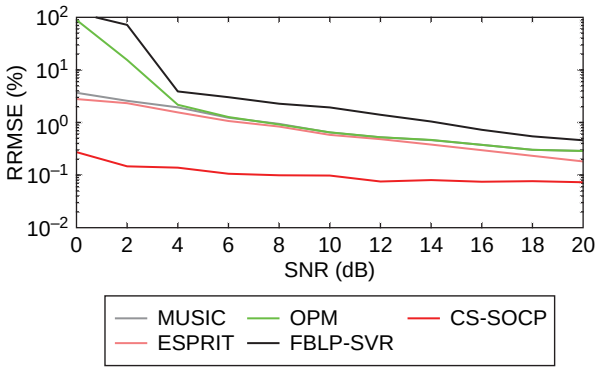

FIGURE 7. The RRMSE of the estimated thickness $\hat{H}$ versus the SNR.

Table 3. The consuming time for a single run with one snapshot on a computer equipped with a CPU of 2.4 GHz and 4 GB of RAM.

Method	Consuming Time		
MUSIC	38.2 ms	8.69 ms for EVD	29.5 ms for 1D search
ESPRIT	23.5 ms	—	—
OPM	28.1 ms	1.85 ms for propagator estimation	26.2 ms for 1D search
FBLP-SVR	33.5 ms	8.75 ms for ω estimation	25.7 ms for 1D search
CS-SOCP	1,320 ms	—	—

High-resolution methods associated with preprocessing techniques (subband averaging techniques) can be adapted to interface roughness estimation [16]. In [16], a modified ESPRIT algorithm is adopted to jointly estimate the time delay and interface roughness. A similar relationship between $\mathbf{A}_{L1}$ and $\mathbf{A}_{L2}$ can be found with $\mathbf{A}_{L2} = \mathbf{A}_{L1}\boldsymbol{\Phi}$, with the $K \times K$ diagonal matrix $\boldsymbol{\Phi} = \text{diag}\{e^{-(2j\pi t_1 + b_1)\Delta f}, \ldots, e^{-(2j\pi t_K + b_K)\Delta f}\}$. According to the principle of ESPRIT [5], the diagonal elements of $\boldsymbol{\Phi}$ can be retrieved from a matrix $\boldsymbol{\Psi}$ that has the same eigenvalues as $\boldsymbol{\Phi}$. Then, the time delay and interface roughness can be estimated by calculating the phase and modulus of the eigenvalues of $\boldsymbol{\Phi}$, respectively.

However, it was found in [15] that, with the widening of the frequency band, the assumption of an exponential frequency behavior is not valid. The frequency behavior can be better approximated by a Gaussian function for GPR with frequency bandwidth $B > 2$ GHz, as $w_k(f) = \alpha_k(f) \approx \exp(-c_k f^2)$, with c_k representing the roughness parameter of the kth interface [15]. When a Gaussian frequency behavior is taken into account in the signal model, conventional subband averaging techniques can no longer be used. In fact, they work only on exponential frequency behaviors [15]. Moreover, methods like machine learning and CS may apply a multidimensional search in roughness estimation, which is computationally inefficient.

In [14] and [15], an interpolated spatial smoothing technique is proposed to interpolate the frequency behavior of the backscattered echoes into an exponential frequency behavior that can take into account several possible frequency behaviors and is suitable for GPR with a large frequency bandwidth. By applying interpolation, a new data covariance matrix can be written as follows:

$$\hat{\mathbf{R}} = \mathbf{B}\mathbf{A}\mathbf{S}\mathbf{A}^H\mathbf{B}^H + \sigma_n^2\mathbf{B}\boldsymbol{\Sigma}\mathbf{B}^H, \tag{17}$$

where $\mathbf{B}$ is the transformation matrix of interpolation [14]. Matrix $\mathbf{B}$ can be computed offline and only once for any interface. Then, subband averaging techniques are applied on $\hat{\mathbf{R}}$ to decorrelate the echoes, making the estimation of the time delay and interface roughness possible. For example, in [15], a modified MUSIC algorithm based on the Rayleigh quotient is proposed for a large frequency bandwidth ($B > 2$ GHz). It allows estimating the time delays without knowing the frequency behavior. The interface roughness can then be estimated by using the maximum likelihood method.

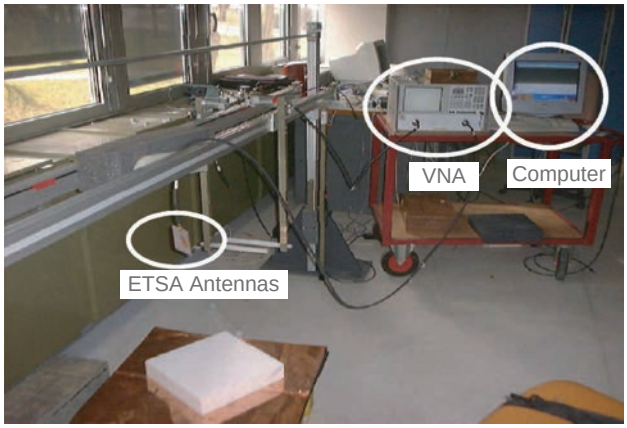

FIGURE 8. IFSTTAR experimental devices, consisting of a VNA. ETSA antennas, and a computer [9].

Thickness estimation in dispersive media

In low-loss media with smooth interfaces, the received signal is modeled as the sum of some time-shifted and attenuated copies of the transmitted signal. Nevertheless, this model does not hold for lossy and dispersive media, so the aforementioned signal processing techniques can no longer work. Some modifications should be made on both the model and methods.

To consider the effects of propagation in dispersive media, the constant-Q model was proposed [7]. This framework applies a complex power function of frequency for the media permittivity. Similar to the signal model in roughness estimation, the constant-Q model is a nonlinear one. Accordingly, the interpolation procedure in (17) should be used, but with a different transformation matrix $\mathbf{B}$ that contains information of the time delays and Q factor. In [7], a modified matrix pencil method, combined with a spline interpolation technique, is proposed to estimate the time delays, permittivity, Q factor, and, consequently, the thickness. It applies an iterative procedure to rebuild the Vandermonde structure of the mode matrix.

In thickness estimation, future work may consider both media dispersion and interface roughness in the signal model, which will make the estimation more realistic but more complex. New methods might also be proposed for this new signal model.

Experimental examples

This section is devoted to thickness estimation by GPR measurement. The experimental setup is shown in Figure 8. A monostatic step-frequency radar is used, which is composed of a vector network analyzer (VNA) and an antenna device whose transmitter and receiver are allocated together. The exponential tapered slot antennas (ETSA) [9] are used for both transmitter and receiver, which are set 70 cm above the tested materials, as shown in Figure 9.

In Figure 9, a smooth polyvinyl chloride (PVC) slab is probed, which is set on a metal plane. The GPR frequency bandwidth ranges from 1.6 GHz to 3.2 GHz, with a 0.02 GHz frequency step (81 frequency samples). Therefore, the roughness can be ignored. The thickness of the PVC is approximately 4 cm, with a relative permittivity $\varepsilon_r = 2.97 + 0.015j$. The relative permittivity is obtained from a data sheet [30], which can be measured by a coaxial cylindrical EM cell. In this situation, the probed material can be considered as a low-loss medium [2], and the medium dispersive can then be neglected. Thus, the frequency behavior $w(f) \approx 1$. The radar pulse is measured with a metal plane [5]. To calculate the thickness of the PVC, only the time delays of the echoes needs to be estimated.

By applying the preprocessing methods—filtering (to eliminate the echoes received outside the GPR main working time window) and data whitening (to whiten the data by radar pulse)—the preprocessed data are obtained [see Figure 10(a)]. As shown in that graph, the black line indicates the

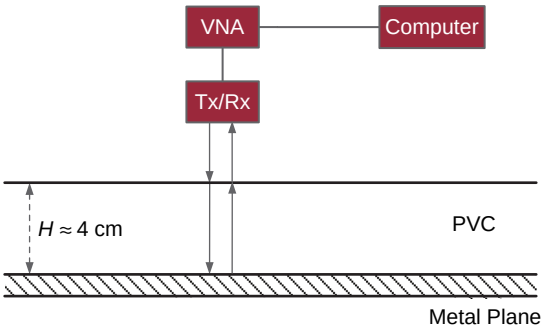

(a)

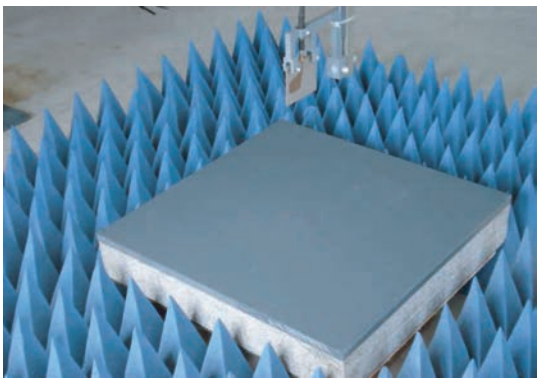

(b)

FIGURE 9. The studied medium—a smooth PVC slab [9]: (a) a diagram of the setup and (b) a photo of the actual layout. Tx: transmitter; Rx: receiver.

preprocessed data, and the red dashed line the envelopes calculated by the Hilbert transform, which provides the analytic representation of the received signal. It can be seen that the backscattered echoes are overlapped and cannot be detected. Therefore, high-resolution methods are required. In the experiment, two subspace-based techniques (MUSIC and ESPRIT [5]), a propagator-based approach (OPM [25]), and a machine-learning method (FBLP-SVR [10]) are tested for TDE.

Table 4 and Figure 10(b) provide the experimental results of the applied methods. In a real measurement, there are, generally, no true values available for the estimated thickness. However, the applied methods share similar results; the estimated thicknesses are within the interval $[4.09, 4.19]$ cm, which are acceptable in thickness estimation (the thickness of the PVC is approximately 4 cm).

Conclusions and future perspectives

In this article, we take a broad view of the current development of the signal processing methods used to solve estimation problems of GPR applications in civil engineering. For each application, there are specific signal processing methods with appropriate data preprocessing. The preprocessing methods (basic data processing and subband averaging techniques) help improve the readability of data and make the data close to those of the assumed signal models. Then, high-resolution, machine-learning, and CS-based methods serve as tools for media parameter estimation (thickness, permittivity,

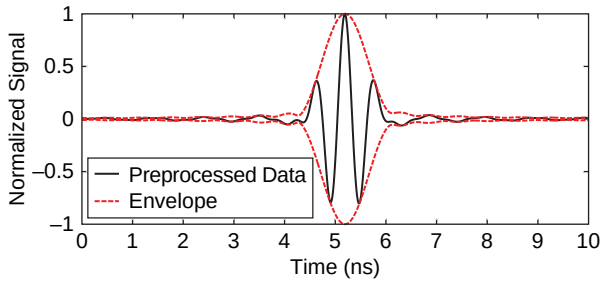

(a)

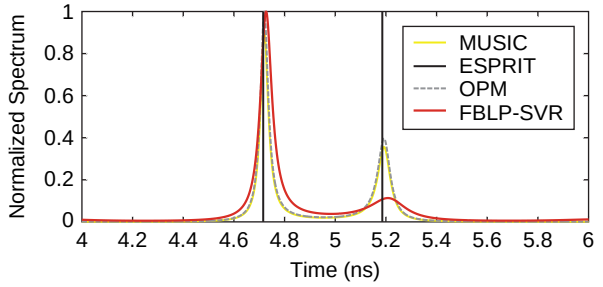

(b)

FIGURE 10. Experimental results: (a) preprocessed data (A-scan) and (b) pseudospectrum.

Table 4. The time delay and thickness estimation.

Method	Estimated Time Delay ($\widehat{\Delta\tau}$)	Estimated Thickness ($\hat{H}$)	Preprocessing Methods
ESPRIT	0.470 ns	4.09 cm	Filtering, data whitening, and subband averaging
MUSIC	0.473 ns	4.12 cm	Filtering, data whitening, and subband averaging
OPM	0.472 ns	4.11 cm	Filtering, data whitening, and subband averaging
FBLP-SVR	0.481 ns	4.19 cm	Filtering and data whitening

and roughness). Experimental examples are presented to test the performance of the representative GPR methods. As GPR measurements are large in data volume, methods with high computational loads may be too time consuming for real-time processing. Therefore, future work may be directed toward to finding the best tradeoff between estimation accuracy and computational complexity for GPR data processing. Artificial intelligence-based techniques with high accuracy that are computationally efficient (with the training procedure done offline) may be a promising future for GPR data processing.

Acknowledgments

We would like to thank the Shanghai Sailing Program (19YF1419100) and the National Natural Science Foundation of China (61701297) for funding part of this work.

Authors

Meng Sun (msun@shmtu.edu.cn) received his B.S. and M.S. degrees from Northwest University, Xi'an, China, and South

China University of Technology, Guangzhou, China, in 2010 and 2013, respectively. He received his Ph.D. degree from IETR Laboratory at Polytech Nantes, Université de Nantes, France, in 2016. He is currently with the Information Engineering College, Shanghai Maritime University, China. His main research focus is signal processing techniques for parameter estimation of civil engineering materials.

Jingjing Pan (jingjing.pan1@etu.univ-nantes.fr) received her B.S. and M.S. degrees in cartography and geographic information science from East China Normal University, Shanghai, and Beijing Normal University, China, in 2012 and 2015, respectively. She received her Ph.D. degree from Polytech Nantes, Université de Nantes, France, in 2018. Her work involves the improvement of signal processing methods with ground-penetrating radar. She is the corresponding author of this article. She is a Member of the IEEE.

Cédric Le Bastard (cedric.lebastard@cerema.fr) received his B.S. and M.S. degrees in electronic engineering from the University of Rennes, France, in 2001 and 2003, respectively, and his Ph.D. degree in electronic engineering from the University of Nantes, France, in 2007. He is currently with the project team ENDSUM at the Centre for Expertise and Engineering on Risks, Environment, Mobility, and Urban and Country Planning, France. He is also a researcher associated with the Institute of Electronics and Telecommunications of Rennes, France. His research interests include radar, nondestructive testing and evaluation, electromagnetic wave scattering, time-delay estimation, and array signal processing.

Yide Wang (yide.wang@univ-nantes.fr) received his B.S. degree in electrical engineering from the Beijing University of Post and Telecommunication, China, in 1985, and his M.S. and Ph.D. degrees in signal processing and telecommunications from the University of Rennes, France, in 1986 and 1989, respectively. He is currently a professor with Polytech Nantes, Université de Nantes, France. His research interests include array signal processing, spectral analysis, and mobile wireless communication systems.

Jianzhong Li (jianzhong.li@gdut.edu.cn) received a Ph.D. degree in signal and image processing from the University of Nantes, France, and a Ph.D. degree in signal and communication engineering from South China University of Technology, Guangzhou, in 2017. He is currently an assistant professor at Guangdong University of Technology, Guangzhou, China. His research interests include array signal processing, image processing, and artificial intelligence.

References

[1] H. M. Jol, *Ground Penetrating Radar Theory and Applications*. Amsterdam, The Netherlands, Elsevier, 2009.

[2] D. J. Daniels, *Ground Penetrating Radar*, 2nd ed. London: IEE Press, 2004.

[3] W. L. Lai, X. Dérobert, and P. Annan, "A review of ground penetrating radar application in civil engineering: A 30-year journey from locating and testing to imaging and diagnosis," *NDT & E Int.*, vol. 96, pp. 58–78, June 2018.

[4] A. Benedetto, F. Tosti, L. B. Ciampoli, and F. D'Amico, "An overview of ground-penetrating radar signal processing techniques for road inspections," *Signal Process.*, vol. 132, pp. 201–209, Mar. 2017.

[5] C. Le Bastard, V. Baltazart, Y. Wang, and J. Saillard, "Thin-pavement thickness estimation using GPR with high-resolution and superresolution methods," *IEEE Trans. Geosci. Remote Sens.*, vol. 45, no. 8, pp. 2511–2519, 2007.

[6] A. P. Annan, N. Diamanti, J. D. Redman, and S. R. Jackson, "Ground-penetrating radar for assessing winter roads," *Geophys.*, vol. 81, no. 1, pp. WA101–WA109, 2015.

[7] K. Chahine, V. Baltazart, and Y. Wang, "Interpolation-based matrix pencil method for parameter estimation of dispersive media in civil engineering," *Signal Process.*, vol. 90, no. 8, pp. 2567–2580, 2010.

[8] M. Solla, R. Asorey-Cacheda, X. Núñez-Nieto, and B. Conde-Carnero, "Evaluation of historical bridges through recreation of GPR models with the FDTD algorithm," *NDT & E Int.*, vol. 77, pp. 19–27, Jan. 2016.

[9] C. Le Bastard, "Apport de techniques de traitement du signal super et haute résolution à l'amélioration des performances du radar chaussée," Ph.D. dissertation, Laboratoire Central des Ponts et Chaussées de Nantes, Univ. Nantes, France, 2007.

[10] J. Pan, C. Le Bastard, Y. Wang, and M. Sun, "Time-delay estimation using ground-penetrating radar with a support vector regression-based linear prediction method," *IEEE Trans. Geosci. Remote Sens.*, vol. 56, no. 3, pp. 2833–2840, 2018.

[11] H. Liu and M. Sato, "In situ measurement of pavement thickness and dielectric permittivity by GPR using an antenna array," *NDT & E Int.*, vol. 64, pp. 65–71, June 2014.

[12] I. L. AL-Qadi and S. Lahouar, "Measuring layer thickness with GPR: Theory to practice," *Construction Building Mater.*, vol. 19, no. 10, pp. 763–772, 2005.

[13] J. S. Lee, C. Nguyen, and T. Scullion, "A novel, compact, low-cost, impulse ground-penetrating radar for nondestructive evaluation of pavements," *IEEE Trans. Instrum. Meas.*, vol. 53, no. 6, pp. 1502–1509, 2004.

[14] M. Sun, C. Le Bastard, Y. Wang, N. Pinel, J. Pan, V. Baltazart, J. M. Simonin, and X. Dérobert, "Time delay and interface roughness estimation using modified ESPRIT with interpolated spatial smoothing technique," *IEEE Trans. Geosci. Remote Sens.*, vol. 56, issue. no. 5, pp. 1475–1484, 2018.

[15] M. Sun, C. Le Bastard, N. Pinel, Y. Wang, J. Li, J. Pan, and Z. Yu, "Estimation of time delay and interface roughness by GPR using modified MUSIC," *Signal Process.*, vol. 132, pp. 272–283, Mar. 2017.

[16] M. Sun, C. Le Bastard, N. Pinel, Y. Wang, and J. Li, "Road surface layers geometric parameters estimation by ground penetrating radar using estimation of signal parameters via rotational invariance techniques method," *IET Radar, Sonar Navigation*, vol. 10, no. 3, pp. 603–609, 2016.

[17] M. Sun, C. Le Bastard, Y. Wang, and N. Pinel, "Time-delay estimation using ESPRIT with extended improved spatial smoothing techniques for radar signals," *IEEE Geosci. Remote Sens. Lett.*, vol. 13, no. 1, pp. 73–77, 2016.

[18] L. Qu, Q. Sun, T. Yang, L. Zhang, and Y. Sun, "Time-delay estimation for ground penetrating radar using ESPRIT with improved spatial smoothing preprocessing," *IEEE Geosci. Remote Sens. Lett.*, vol. 11, no. 8, pp. 1315–1319, 2014.

[19] C. L. Bastard, Y. Wang, V. Baltazart, and X. Dérobert, "Time delay and permittivity estimation by ground-penetrating radar with support vector regression," *IEEE Geosci. Remote Sens. Lett.*, vol. 13, no. 1, pp. 873–877, 2014.

[20] Y. Liu, G. Y. Li, Z. Tan, and H. Hu, "Noise power estimation in SC-FDMA systems," *IEEE Wireless Commun. Lett.*, vol. 4, no. 2, pp. 217–220, 2017.

[21] I. Volaric, V. Sucic, and S. Stankovic, "A data driven compressive sensing approach for time-frequency signal enhancement," *Signal Process.*, vol. 141, pp. 229–239, Dec. 2017.

[22] M. Wax and T. Kailath, "Detection of signals by information theoretic criteria," *IEEE Trans. Acoust., Speech, Signal Process.*, vol. 33, no. 2, pp. 387–392, 1985.

[23] A. Badawy, T. Salman, T. Elfouly, T. Khattab, A. Mohamed, and M. Guizani, "Estimating the number of sources in white Gaussian noise: Simple eigenvalues based approaches," *IET Signal Process.*, vol. 11, no. 6, pp. 663–673, 2017.

[24] E. Radoi and A. Quinquis, "A new method for estimating the number of harmonic components in noise with application in high resolution radar," *EURASIP J. Advances Signal Process.*, vol. 2004, pp. 1177–1188, Jan. 2004.

[25] S. Marcos, A. Marsal, and M. Benidir, "The propagator method for source bearing estimation," *Signal Process.*, vol. 42, no. 2, pp. 121–138, 1995.

[26] M. Pastorino and A. Randazzo, "A smart antenna system for direction of arrival estimation based on a support vector regression," *IEEE Trans. Antennas Propag.*, vol. 53, no. 7, pp. 2161–2168, 2005.

[27] A. C. Gurbuz, J. H. McClellan, and W. R. Scott, "A compressive sensing data acquisition and imaging method for stepped frequency GPRs," *IEEE Trans. Signal Process.*, vol. 57, no. 7, pp. 2640–2650, 2009.

[28] D. Malioutov, M. Cetin, and A. S. Willsky, "A sparse signal reconstruction perspective for source localization with sensor arrays," *IEEE Trans. Signal Process.*, vol. 53, no. 8, pp. 3010–3022, 2005.

[29] J. Yang, T. Jin, X. Huang, J. Thompson, and Z. Zhou, "Sparse MIMO array forward-looking GPR imaging based on compressed sensing in clutter environment," *IEEE Trans. Geosci. Remote Sens.*, vol. 52, no. 7, pp. 4480–4494, 2014.

[30] M. Adous, "Electromagnetic characterization of concrete in the frequency range 50 MHz–13 GHz," Ph.D. dissertation, Laboratoire Central des Ponts et Chaussées de Nantes, Univ. Nantes, France, 2006.